

Far field subwavelength focusing using optical eigenmodes

Jörg Baumgartl,¹ Sebastian Kosmeier,¹ Michael Mazilu,^{1,a)} Edward T. F. Rogers,² Nikolay I. Zheludev,² and Kishan Dholakia¹

¹*SUPA, School of Physics and Astronomy, University of St. Andrews, St. Andrews, North Haugh, Fife KY16 9SS, United Kingdom*

²*Optoelectronics Research Centre and Centre for Photonic Metamaterials, University of Southampton, Highfield, Southampton SO17 1BJ, United Kingdom*

(Received 23 December 2010; accepted 12 April 2011; published online 6 May 2011)

We report the focusing of light to generate a subdiffractive, subwavelength focal spot of full width half maximum 222 nm at an operating wavelength of 633 nm using an optical eigenmode approach. Crucially, the spot is created in the focal plane of a microscope objective thus yielding a practical working distance for applications. The optical eigenmode approach is implemented using an optimal superposition of Bessel beams on a spatial light modulator. The effects of partial coherence are also discussed. This far field method is a key advance toward the generation of subdiffractive optical features for imaging and lithographic purposes. © 2011 American Institute of Physics. [doi:10.1063/1.3587636]

The diffraction limit has been thought to impose a fundamental limit on the resolution of focusing and imaging for over a century. However, research over the past decade has explored methods to overcome this limitation. Significant attention has focused on near field strategies to recover non-propagating evanescent waves whose range of k vectors are required to reduce the size of a focal spot below the diffraction limit. Near-field techniques such as scanning near-field optical microscopy (SNOM) (Refs. 1 and 2) and the use of field concentrators^{3–6} have been explored. The concept of a superlens^{7–10} is still visionary being based on suitable bulk metamaterials which are still to be developed. While the near field has seen most activity, in general, concepts to beat the diffraction limit in the far-field are still rare and have only recently been realized in the optical domain using either a lensless angular spectrum synthesis approach¹¹ or nanohole arrays.^{12,13} The latter split and reinterfere light fields to subdiffraction-limited hot spots at a typical distance of 10 μm from the array. Nanohole arrays exploit the fundamental concept of superoscillations^{14,15} which states that a band-limited function may oscillate faster than its highest Fourier component. This is achieved through a redistribution of intensity from high-frequency to low-frequency modes. In the case of optical fields, this means that the size of a focal spot may arbitrarily be reduced at the expense of the spot intensity and the emergence of sidebands which contain the vast majority of the optical intensity.¹⁶ It would be immensely advantageous to show how we may squeeze light in the far field to beat the diffraction limit while retaining a useable working distance. Indeed, even a factor of 2 resolution improvement greatly enhances the imaging capabilities in microscopy.¹⁷ The advantages would be further enhanced if we were able to achieve this using readily available technology.

Here, we show the generation and study the stability of subwavelength focal spots in the “far-field” regime. More precisely, we use the optical eigenmode technique^{16,18} to determine the minimum spot size achievable in the focal plane

of a microscope objective and for a given region of interest (ROI). This is a powerful, “far-field” method and constitutes a significant step forward toward the application of subwavelength spots in super-resolving imaging and lithographic devices. A spatial light modulator (SLM) was used to create the optical eigenmode beam which allows us to generate the subdiffractive spot as an optimized superposition of Bessel beams (BBs). Moreover, we remark that the optimization procedure, as implemented here, is compatible with any optical microscope system bringing subdiffractive focal spots readily within reach of numerous applications.

Theory. In order to reduce the spot size below the subwavelength diffraction limit we employed the optical eigenmode method as reported by Mazilu *et al.*¹⁶ In brief, a number of N test fields $u_n(x, y) = A_n(x, y) \exp[i\phi_n(x, y)]$, $n = 1, \dots, N$ serves to construct the finite intensity $\mathbf{M}^{(0)}$ and second order momentum $\mathbf{M}^{(2)}$ operators for a given lateral ROI. The individual elements of this matrix operator are given by $M_{mn}^{(0)} = \int_{\text{ROI}} u_m^* u_n da$ and $M_{mn}^{(2)} = \int_{\text{ROI}} r^2 u_m^{(0)*} u_n^{(0)} da$ where r is the distance from the origin. The eigenmode with the smallest eigenvalue of $\mathbf{M}^{(2)}$ represented in the normalized eigenmode base of $\mathbf{M}^{(0)}$ corresponds to the smallest achievable spot for the given ROI and test fields.

Experimental setup. We used a standard first-order holographic microscopy arrangement (as typically used for optical-tweezers).¹⁹ The beam of a 10 mW HeNe laser ($\lambda = 633 \text{ nm}$) was expanded in order to slightly overfill a phase-only SLM (Holoeye, HEO 1080 P) where the maximum circular chip area (diameter of 1080 pixel) was used to modulate the incident beam. The beam was then imaged onto the back aperture of a microscope objective (Nikon 40 \times , 0.65 NA) through a pair of lenses. The objective focuses an unmodulated Gaussian beam to the diffraction-limited Airy disk with a full width at half maximum (FWHM) of $w_0 = 0.5\lambda/\text{NA} \approx 488 \text{ nm}$. We imaged the fields created in the focal plane of the objective with a SNOM tip (30 nm in diameter). The tip was fiber-coupled to a photomultiplier tube which, in turn, was connected to a lock-in amplifier where the required reference signal was provided by chopping the laser beam at a rate of 6 kHz using a chopper wheel.

^{a)}Electronic mail: michael.mazilu@st-andrews.ac.uk.

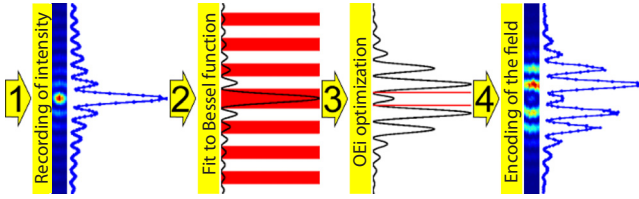


FIG. 1. (Color online) Four-step optimization procedure. Step 1: Determination of the 1D intensity cross section (r.h.s) from measured set of 2D intensity profiles of BBs (l.h.s). Step 2: Fit function to 1D cross sections. The continuous curve is the fitted intensity cross section. White and shaded bars indicate the associated phase profile (white=0, shaded= π). Step 3: Optical eigenmode (OEI) optimization. The horizontal lines indicate a range of interest as used for the optimization procedure. Step 4: implementation and characterization of the final optimized mask.

Experimental procedure. As probing fields, we used fifteen BBs (BB1 to BB15) each created by applying an annulus modulation to the SLM display. The optical eigenmode method was implemented experimentally through a four-step procedure as visualized in Fig. 1. A one-dimensional (1D) cross section through each BB center was extracted from the two-dimensional (2D) intensity profiles (see Fig. 1, step 1: 2D profile on the l.h.s., 1D cross section on the r.h.s.). In step 2, we fitted the function $f(x)=J_0(x/x_0)^2$ to the measured 1D cross sections where J_0 denotes the zero-order Bessel function and x_0 a transverse characteristic length scale. Explicit values are provided in Table I for the selected BBs along with information on the FWHM. The phase of each beam was implicitly determined through the procedure for wave front correction applied prior to the optimization.²⁰ In step 3, the eigenmode optimization (described in the theoretical paragraph above) is performed using the intensity eigenmodes with eigenvalues above a threshold intensity T . The optimization step determines the complex valued amplitudes of the 15 BBs delivering the smallest spot. This superposition of BBs can be created with the phase-only SLM using the approach reported by Davis *et al.*²¹ We remark that two SLMs may also be used to decouple the amplitude and phase modulation respectively.¹⁶ The resulting field distribution is finally characterized and compared to the theoretical prediction in step 4. The overall procedure is relatively fast (30 min), where the time duration is limited by the scanning stage.

Results. The results presented in Fig. 2 are based on a superposition of the BB probe fields which predicted a focal spot with a FWHM smaller than $\lambda/2$ for the ROI size smaller than the wavelength. The threshold T was set to a value 2000 times smaller than the total intensity of BB1 within the ROI. The subdiffractive spot was then approximately five times less intense than the side bands. Figure 2 shows the focal spot field distribution which we realized in our experiments for a ROI size of 507 nm. The ROI size is indicated by the two red lines in the bottom graph of Fig. 2(a) which shows

TABLE I. Airy disk (AD) and test BB parameters. x_0 is a characteristic transverse length scale of the test BBs.

Beam	AD	BB 1	BB 8	BB 15
FWHM (nm)	488	366	590	1464
FWHM (λ)	0.77	0.57	0.93	2.31
x_0 (nm)	...	1036	1684	4212

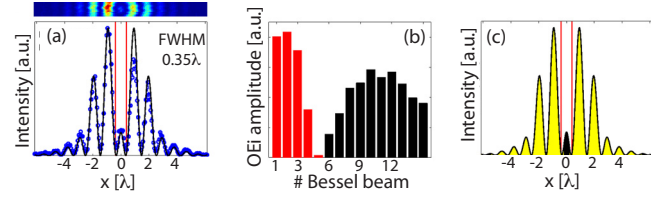


FIG. 2. (Color online) Subdiffraction-limited focal spot. (a) Top: 2D intensity profile, bottom: 1D intensity cross-section, measured (dots), theoretical prediction (continuous curve). Vertical lines indicate the ROI size 0.76λ . (b) Optical eigenmode amplitudes for BB1 to BB15. Phase shift indicated by shade: zero (black bar), π (gray bar). (c) The superoscillatory region is identified in black.

the theoretical predicted intensity distribution as a black line curve and the actually measured distribution as a blue scatter-line curve. The top part of Fig. 2(a) shows the associated measured 2D intensity distribution. Data evaluation yielded a focal spot FWHM of 222 nm which is 35% of the laser wavelength, 45% of the corresponding diffraction-limited Airy disk, and 60% of the FWHM of BB1, the test beam featuring the smallest core FWHM of all 15 BB test fields. Figure 2(b) provides information on how the final optimized distribution is assembled from the individual test BBs. Every BB significantly contributes except for BB5 and BB1 to BB5 are out of phase by π with respect to BB6 to BB15. We remark that the realized focal spot pattern exhibited superoscillatory behavior which manifests itself in a local wave vector which is larger than the wave vectors supported by the spectral density of the hot spot field distribution.²² The local wave vector was determined as $\partial_r \arg u(r)$ where u denotes the analytical complex field. The outcome of the superoscillation analysis is shown in Fig. 2(c) where superoscillatory regions are identified using black color area filling within the field distribution. The focal spot clearly exhibits superoscillatory behavior though with only 1% of the Airy disk peak intensity.

Stability study. For practical applications, an important question is that of the behavior of the smallest spot eigenmode when perturbed. One method to simulate this behavior is via the Gaussian shell model describing the propagation of partially coherent light.²³ Using this formalism, we have numerically simulated the effect of the loss of spatial coherence upon the smallest spot size achievable. Figure 3 shows the evolution of the Airy disk (red) and smallest spot eigenmode optimized for perfectly coherent light (blue). We remark that

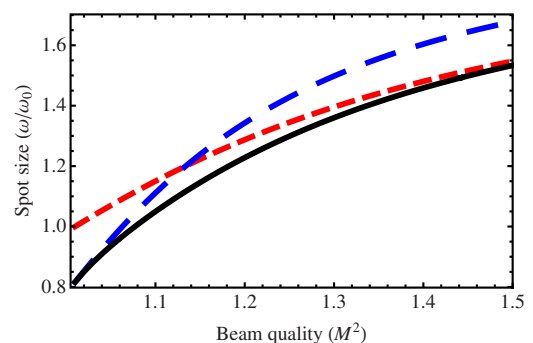


FIG. 3. (Color online) Numerical simulation of the spot size as a function of the incident beam quality factor M^2 for three different beam profiles: (short dashed) Airy disk, (long dashed) smallest spot optical eigenmode, and (continuous) smallest spot optical eigenmode taking into account the partial coherence length.

both spots increase in size with the eigenmode spot losing its initial advantage faster than the Airy disk. This can be understood through the “diffusion” of the sidebands into the ROI destroying the subwavelength spot as the light field loses coherence. Figure 3 also shows an optical eigenmode (black) that minimizes the spot size taking into account the precise coherence length of the incident light. This is possible as the description of the intensity within the Gaussian shell model remains quadratic with respect to the field. We observe that for any given degree of coherence there exists an eigenmode beam that focuses light to a smaller spot than the corresponding Airy disk and thus correcting for the loss of coherence.

Conclusion. In conclusion, we have reported the controlled generation of subwavelength and subdiffractive light fields using an optical eigenmode approach implemented with an SLM and an optical microscope. Employing the eigenmode optimization, we may indeed squeeze a focal spot to the subdiffraction, subwavelength regime and achieve a spot size of 35% of the laser wavelength. Our optimal superposition of BBs not only beats the Airy disk but also any individual BB diameter. Our methodology may readily be implemented in any optical microscopy system.

We thank the UK Engineering and Physical Sciences Research Council for funding (grant EP/F040644/1) and Mark Dennis for helpful discussions. K.D. is a Royal Society Wolfson Merit Award Holder.

- ¹E. Betzig, J. K. Trautman, T. D. Harris, J. S. Weiner, and R. L. Kostelak, *Science* **251**, 1468 (1991).
- ²A. Hartschuh, E. J. Sanchez, X. S. Xie, and L. Novotny, *Phys. Rev. Lett.* **90**, 095503 (2003).
- ³K. Li, M. I. Stockman, and D. J. Bergman, *Phys. Rev. Lett.* **91**, 227402 (2003).
- ⁴M. I. Stockman, *Phys. Rev. Lett.* **93**, 137404 (2004).
- ⁵R. Merlin, *Science* **317**, 927 (2007).
- ⁶A. Grbic, L. Jiang, and R. Merlin, *Science* **320**, 511 (2008).
- ⁷J. B. Pendry, *Phys. Rev. Lett.* **85**, 3966 (2000).
- ⁸A. Salandrino and N. Engheta, *Phys. Rev. B* **74**, 075103 (2006).
- ⁹Z. Jacob, L. V. Alekseyev, and E. Narimanov, *Opt. Express* **14**, 8247 (2006).
- ¹⁰Z. Liu, H. Lee, Y. Xiong, C. Sun, and X. Zhang, *Science* **315**, 1686 (2007).
- ¹¹S. S. Hong, K. P. Berthold, D. M. Freeman, and M. S. Mermelstein, *Appl. Phys. Lett.* **88**, 261107 (2006).
- ¹²F. M. Huang, N. I. Zheludev, Y. Chen, and F. J. Garcia de Abajo, *Appl. Phys. Lett.* **90**, 091119 (2007).
- ¹³F. M. Huang, T. S. Kao, V. A. Fedotov, Y. Chen, and N. I. Zheludev, *Nano Lett.* **8**, 2469 (2008).
- ¹⁴M. V. Berry and S. Popescu, *J. Phys. A* **39**, 6965 (2006).
- ¹⁵F. M. Huang and N. I. Zheludev, *Nano Lett.* **9**, 1249 (2009).
- ¹⁶M. Mazilu, J. Baumgartl, S. Kosmeier, and K. Dholakia, *Opt. Express* **19**, 933 (2011).
- ¹⁷M. G. L. Gustafsson, *J. Microsc.* **198**, 82 (2000).
- ¹⁸M. Mazilu, *J. Opt. A, Pure Appl. Opt.* **11**, 094005 (2009).
- ¹⁹K. Dholakia, P. J. Reece, and M. Gu, *Chem. Soc. Rev.* **37**, 42 (2008).
- ²⁰T. Čižmár, M. Mazilu, and K. Dholakia, *Nat. Photonics* **4**, 388 (2010).
- ²¹J. A. Davis, D. M. Cottrell, J. Campos, M. J. Yzuel, and I. Moreno, *Appl. Opt.* **38**, 5004 (1999).
- ²²M. R. Dennis, A. C. Hamilton, and J. Courtial, *Opt. Lett.* **33**, 2976 (2008).
- ²³S. C. H. Wang and M. A. Plonus, *J. Opt. Soc. Am.* **69**, 1297 (1979).